Gamma-ray spectra due to cosmic-ray interactions with dense gas clouds

Michiko Ohishi, Masaki Mori

Institute for Cosmic Ray Research, University of Tokyo, Kashiwa, Chiba 277-8582, Japan

&

Mark Walker

School of Physics, University of Sydney, NSW2006, Australia
Australia Telescope National Facility, CSIRO, Australia

ABSTRACT

Gamma-ray spectra from cosmic-ray proton and electron interactions with dense gas clouds have been calculated using a Monte Carlo event simulation code, GEANT4. Such clouds are postulated as a possible form of baryonic dark matter in the Universe. The simulation fully tracks the cascade and transport processes which are important in a dense medium, and the resulting gamma-ray spectra are computed as a function of cloud column-density. These calculations are used for predicting the Galactic diffuse gamma-ray spectrum which may be contributed by baryonic dark matter; the results are compared with data from the EGRET instrument, and used to constrain the fraction of Galactic dark matter which may be in the form of dense gas clouds. In agreement with previous authors, we find useful constraints on the fraction of Galactic dark matter which may be in the form of low column-density clouds ($\Sigma \lesssim 10\,\mathrm{g\,cm^{-2}}$). However, this fraction rises steeply in the region $\Sigma \sim 10^2\,\mathrm{g\,cm^{-2}}$, and for $\Sigma \gtrsim 200\,\mathrm{g\,cm^{-2}}$ we find that baryonic dark matter models are virtually unconstrained by the existing gamma-ray data.

Subject headings: gamma-rays — cosmic rays — ISM: clouds — dark matter

1. Introduction

The nature of dark matter remains one of the outstanding questions of modern astrophysics. The success of the cold dark matter cosmological model (albeit with "dark energy" now required: ΛCDM) argues strongly for a major component of the dark matter being in the form of an elementary particle. However, the inventory of baryons which we can observe locally falls far short of the total inferred from observations of the cosmic microwave background fluctuations (Fukugita 2004), leaving open the possibility that there may be a significant baryonic component of dark matter. Furthermore, although ΛCDM is very successful in describing the growth of structure in the universe on large scales, we still lack a direct detection of any of the candidate dark matter particles. Lacking this decisive piece of observational evidence, some authors have proposed models which include a large component of baryonic dark matter. In particular there have been many papers dealing with the possibility that cold, self-gravitating molecular clouds constitute a major component of the dark matter (Pfenniger, Combes and Martinet 1994; De Paolis et al. 1995; Henriksen and Widrow 1995; Gerhard and Silk 1996; Combes and Pfenniger 1997; Walker 1999; Sciama 2000a,b). A variety of different forms, including isolated, clustered, and fractal, have been considered for the clouds, but all proposals involve dense gas of high column-density, in contrast to the diffuse gas in

the interstellar medium which is easily detected in emission and/or absorption.

One of the fundamental predictions of a model featuring dense gas clouds is the gamma-ray emission resulting from cosmic-ray interactions within the clouds (De Paolis et al. 1995; Kalberla, Shchekinov and Dettmar 1999; Wardle and Walker 1999; Sciama 2000a). Because of the potentially large total mass of gas involved, this process may yield a diffuse flux in the Galactic plane comparable to the flux from known sources for photon energies around 1 GeV (Sciama 2000a). Considering the high quality data on diffuse emission acquired by the EGRET detector aboard the Compton Gamma Ray Observatory (Hunter et al. 1997), it is worth considering this source of gamma-ray emission in detail as it is possible to use these data to constrain the dark matter models (see Salati et al. (1996); Gilmore (1994)). Most previous investigations of this problem have neglected the self-shielding and cascade phenomena which can be important at high column densities (Kalberla, Shchekinov and Dettmar 1999; Sciama 2000a), and have employed emissivities appropriate to the low-density limit. These effects alter the emergent gamma-ray spectrum, and we note that this could be relevant to the observed excess Galactic flux above 1 GeV (Hunter et al. 1997). We have noted elsewhere (Walker, Mori and Ohishi 2003) that massive ($M \gtrsim 10^6$ M$_\odot$) aggregates of dense gas clouds could potentially account for many of the unidentified discrete sources detected by EGRET (Hartman et al 1999).

Here we present detailed calculations of the gamma-ray spectra arising from cosmic-ray interactions with dense gas clouds. We have used a Monte Carlo simulation code, GEANT4, developed for simulating interaction events in detectors used in high-energy particle physics. Not surprisingly, we find that the predicted spectra differ substantially between high and low column-density clouds, and we discuss the interpretation of our results in the context of the observed Galactic gamma-ray emission. Our calculations are undertaken for cold, dense molecular gas in clouds of radius $R \sim 10^{13}$cm, similar to those proposed by Walker and Wardle (1998) to explain the extreme scattering events (Fiedler et al. 1994) during which compact extragalactic radio sources are magnified and demagnified as a plasma "lens"

moves across the line of sight (see McKee (2001) for a criticism of this model). However, the results of our calculations depend primarily on the column-density of the individual clouds, Σ, under consideration, and their fractional contribution to the Galaxy's dark matter halo, and our results can be taken as representative of other models which are characterised by similar values of these quantities.

2. Results

2.1. Gamma-ray production in dense gas

Previous calculations of gamma-ray spectra from cosmic-ray irradiation assumed single interactions of protons with the interstellar medium (Stephens and Badhwar (1981); Dermer (1986); Bertsch et al. (1993) and references therein). In order to investigate cosmic-ray interactions with dense gas, where cascade processes and particle transport are important, we have used a Monte Carlo code, GEANT4,[1] to derive gamma-ray production spectra. This code is a general purpose Monte Carlo code of particle interactions and is widely used for simulation of high-energy particle detectors in accelerator experiments. Cross-sections and interactions of various hadronic processes, i.e., fission, capture, and elastic scattering, as well as inelastic final state production, are parametrized and extrapolated in high and low particle energy limits, respectively. The π^0 production in this code, which is important because of the $\pi^0 \to 2\gamma$ decay that dominates the emissivity of the gas at high energies, has been tested against accelerator data (Dannheim 1999).

Initially we experienced one slight difficulty in applying GEANT4 to our physical circumstance: the low-energy hadron interaction code, called GHEISHA, did not conserve energy very accurately (GEANT4 bug reports No. 171 and 389). A "patch" was available for GHEISHA (GEANT ver. 4.4.1), but this patch appeared to introduce further problems of its own in the energy deposition distribution (GEANT4 bug report No. 415). These difficulties have been overcome by the GEANT team, and we are not aware of any such problems in the latest release (GEANT ver. 4.5.1).

---

[1] Available at http://wwwinfo.cern.ch/asd/geant4/geant4.html

Our calculations assume a spherical cloud of molecular hydrogen of uniform density and temperature (10 K). The radius of the sphere was assumed to be $R = 1.5 \times 10^{13}$ cm $\simeq 1$ AU. Protons and electrons are injected randomly at a surface point of the cloud and particles subsequently emanating from this surface are counted as products. The adopted spectra of cosmic-ray protons and electrons were taken from Mori (1997) (here we use the "median" flux; note that the units on his equation (3) should read $\mathrm{cm}^{-2}\mathrm{s}^{-1}\mathrm{sr}^{-1}\mathrm{GeV}^{-1}$), and Skibo and Ramaty (1993), respectively. In Figs. 1 and 2 we plot these spectra together with observational data. (Note that the adopted spectra are those for cosmic rays in the Galaxy, whereas the measured points are subject to the modulating influence of the magnetic field of the solar wind). The simulated range of kinetic energy of cosmic rays is from 10 MeV to 10 TeV. We divided this energy range into four and superposed the resulting spectra with appropriate weight factors in order to increase the simulation statistics at higher energies, considering the rapidly falling spectrum of cosmic rays. The density of molecular hydrogen, ϱ, was varied from 5×10^{-16} to 5×10^{-9} g cm^{-3} in factors of 10. This corresponds to the column density, $\Sigma = 2\varrho R \langle \cos\theta \rangle$, of $10^{-2}, 10^{-1}, \ldots 10^5$ g cm^{-2}, respectively, where θ is the incident angle of a cosmic ray into a cloud and $\langle \cos\theta \rangle = 2/3$ for random injection.

2.2. Simulations

Figure 3 shows the resulting gamma-ray spectra obtained in our GEANT4 simulation for proton injection into a cloud of column density $\Sigma = 100$ g cm^{-2}. (The quantity plotted is $E^2\mathcal{E}$, with $\mathcal{E}$ being the emissivity as given in §3.) The dashed, dotted and dot-dashed lines show the spectral components classified by the parent processes producing gamma-rays, i.e., π^0 decay, bremsstrahlung and positron-electron annihilation, respectively. The latter two components are necessarily omitted in calculations which assume single interactions only (i.e. the thin material limit). The error bars are calculated from Monte Carlo statistics. Although the π^0 decay component shows a broad peak at $E \simeq 70$ MeV (note that the quantity plotted is the emissivity multiplied by E^2) and dominates above about 200 MeV, the electron bremsstrahlung component broadens the emissivity peak. The bremsstrahlung and annihilation contributions are negligible in the limit of small column-density; their fractional contribution to the emission is greatest for clouds which are just thick enough ($\Sigma \sim 10^2 - 10^3$ g cm^{-2}) to attenuate the bulk of the incident proton power. This is as expected considering that the interaction mean free path of GeV protons is ~ 80 g cm^{-2} and is in accordance with the result of Umebayashi and Nakano (1981) who treated a similar problem by solving one-dimensional transport equations.

The resulting gamma-ray emissivities for clouds of various column densities are shown in figure 4 (proton injection) and figure 5 (electron injection). Here the emissivities are defined for irradiation by cosmic-rays of all species (see §2.3, equation (3)); to take account of the contribution of heavier nuclei than helium, the emissivity due to proton irradiation (figure 4) has been multiplied by a nuclear enhancement factor (Cavallo and Gould 1971; Stephens and Badhwar 1981; Dermer 1986; Gaisser and Shaefer 1992) of 1.52 (Mori 1997). Note that for high densities the Monte Carlo statistics are rather poor, since the yield itself is low. Figure 4 includes a comparison of our calculated gamma-ray production functions with that of Mori (1997) (corresponding to the "thin material" limit). The results are consistent with those of Mori (1997) for column densities less than about 10 g cm^{-2}, except in the energy range $E > 10^6$ MeV where the effect of the maximum energy assumed in the Monte Carlo simulation is evident. We note the very low values of the emissivity at energies $\gtrsim 100$ MeV, for column densities $\Sigma \gtrsim 10^3$ g cm^{-2}. A slightly steeper spectrum in the 10^4–10^6 MeV region comes from our omission of the contribution of heavy nuclei, which were taken into account in Mori (1997). A somewhat surprising feature of these curves is that the power-law index above 1 GeV is almost the same as the input cosmic-ray proton flux for column densities less than about 1000 g cm^{-2} (for higher column densities the statistics of the simulations are not good enough to decide whether this result still holds). This is already indicated by Umebayashi and Nakano (1981), but is contrary to the expectation of Sciama (2000a) who suggested a spectral change above 1 GeV at the point where self-shielding becomes important.

For some purposes the energy-integrated emis-

sivities are of more interest than their differential counterparts, so we present these quantities in figures 6 and 7, for cosmic ray protons and electrons, respectively. At low column densities, where cascades and self-shielding are unimportant, there is very little variation of the integrated emissivity with cloud column density, and the thin material limit can be adopted for columns less than $10 \mathrm{\ g\,cm^{-2}}$ for protons ($1 \mathrm{\ g\,cm^{-2}}$ for electrons). Above this point, however, the emissivity drops rapidly with increasing cloud column-density. In order to gauge the sensitivity of these calculations to the assumed cosmic-ray spectra, we have computed our results for two different incident cosmic-ray proton spectra, and three different incident cosmic-ray electron spectra, as shown in figures 6 and 7, respectively. The differences are seen to be small in comparison with the variation as a function of cloud column density, but at a fixed column-density the systematic uncertainties associated with the input cosmic-ray spectra are nevertheless significant.

2.3. Computation of gamma-ray intensities

Using the gamma-ray production spectra obtained in the previous section, we have calculated the diffuse gamma-ray emission from the Galaxy as follows. The predicted gamma-ray spectrum for each case is

$$I_D = \frac{1}{\Sigma} \int_0^\infty \mathrm{d}s\, \rho(s) J_{\mathrm{cr}}(s) \frac{\mathrm{d}N}{\mathrm{d}E} \qquad (1)$$

where $\mathrm{d}N/\mathrm{d}E$ is the spectrum returned by the simulation in units of photons/MeV/primary, for an individual cloud, appropriate to the incident cosmic-ray spectrum. The quantity $J_{\mathrm{cr}}(s)$ is the intensity of cosmic rays at a distance s along the line of sight, in units of primaries $\mathrm{cm^{-2}\ s^{-1}\ sr^{-1}}$, and $\rho(s)$ is the mean density in gas clouds of column density Σ.

The Galactic variation of the spectrum $J_{cr}(s)$ is not well constrained by existing data, and consequently we adopt the simplifying assumption that the shape of the cosmic-ray spectra (both electrons and protons) is the same everywhere in the Galaxy, with variations only in the normalisation. With this assumption it is convenient to recast the calculation as

$$I_D = \frac{1}{4\pi} \mathcal{E} Q, \qquad (2)$$

Table 1: Integrated gamma-ray emissivities of dense gas clouds, due to cosmic-ray hadrons and electrons; these results assume Mori's (1997) "median" proton spectrum and Skibo and Ramaty's (1993) electron spectrum. A nuclear enhancement factor of 1.52 has been applied to the emissivities computed for cosmic-ray protons in order to account for heavier nuclei. Column-densities (Σ) are given in units of $\mathrm{g\,cm^{-2}}$ and integrated emissivities in units of $\mathrm{photons\,s^{-1}g^{-1}}$; photon energies ($E$) are given here in MeV.

Σ	$\int_{100}^{\infty}\mathrm{d}E\,\mathcal{E}$	$\int_{300}^{500}\mathrm{d}E\,\mathcal{E}$	$\int_{1000}^{\infty}\mathrm{d}E\,\mathcal{E}$
10^{-2}	1.47×10^{-1}	2.36×10^{-2}	8.22×10^{-3}
10^{-1}	1.50×10^{-1}	2.34×10^{-2}	1.14×10^{-2}
10^{0}	1.51×10^{-1}	2.61×10^{-2}	9.63×10^{-3}
10^{1}	1.34×10^{-1}	2.15×10^{-2}	9.26×10^{-3}
10^{2}	5.66×10^{-2}	9.04×10^{-3}	3.55×10^{-3}
10^{3}	5.16×10^{-3}	8.43×10^{-4}	3.42×10^{-4}
10^{4}	6.82×10^{-5}	7.11×10^{-6}	4.81×10^{-7}
10^{5}	6.65×10^{-6}	6.90×10^{-7}	3.71×10^{-8}

Table 2: Gamma-ray emissivities of dense gas clouds, due to cosmic-ray hadrons and electrons; these results assume Mori's (1997) "median" proton spectrum, and Skibo and Ramaty's (1993) electron spectrum. A nuclear enhancement factor of 1.52 has been applied to the emissivities computed for cosmic-ray protons, in order to account for heavier nuclei. Column-densities (Σ) are given in units of $\mathrm{g\,cm^{-2}}$, and emissivities in units of $\mathrm{MeV\,s^{-1}g^{-1}}$; photon energies ($E$) are given here in MeV. The quantity $\mathcal{L} \equiv \mathrm{Log}_{10}(E^2 \mathcal{E})$.

$E =$	10	100	1000	10000
Σ	$\mathcal{L}$	$\mathcal{L}$	$\mathcal{L}$	$\mathcal{L}$
10^{-2}	0.889	1.086	1.126	0.657
10^{-1}	0.924	1.059	1.198	0.763
10^{0}	0.824	1.030	1.171	0.594
10^{1}	0.497	0.961	1.145	0.598
10^{2}	-0.223	0.584	0.745	0.164
10^{3}	-1.356	-0.481	-0.276	-0.869
10^{4}	-3.234	-2.175	-2.811	-4.628
10^{5}	-4.251	-3.207	-3.928	-6.024

$(\mathrm{ph\,cm^{-2}s^{-1}sr^{-1}MeV^{-1}})$, where the emissivity is

$$\mathcal{E} = \frac{4\pi}{\Sigma} J_{\mathrm{cr}}(\odot)\frac{\mathrm{d}N}{\mathrm{d}E} \qquad (3)$$

$(\mathrm{ph\,s^{-1}MeV^{-1}g^{-1}})$ with $J_{cr}(\odot)$ the cosmic-ray mean intensity in the Solar neighbourhood and

$$Q \equiv \int_0^\infty \mathrm{d}s\, \rho(s)\frac{J_{\mathrm{cr}}(s)}{J_{\mathrm{cr}}(\odot)} \qquad (4)$$

is the weighted column density $(\mathrm{g\,cm^{-2}})$ of the cloud population along the line-of-sight under consideration. This formulation is convenient because the emissivity, $\mathcal{E}$, describes the properties of the gas clouds themselves and is independent of the Galactic variations in mean dark matter density and cosmic-ray density; conversely the quantity Q characterises these properties of the Galaxy, and is independent of the properties of the gas clouds themselves. The emissivity shown in figures 4 and 5 is the quantity $E^2\mathcal{E}$, whereas figures 6 and 7 show $\int_E^\infty \mathrm{d}E'\,\mathcal{E}$. For the inner Galactic disk, where we are interested in $\langle I_D \rangle$, we need to average over the whole solid angle, Ω, under consideration: $\langle Q \rangle = \int \mathrm{d}\Omega\, Q\,/\Omega$. In order to calculate Q we need to adopt models for both the Galactic cosmic-ray distribution and the Galactic distribution of the clouds.

The quantity $\rho(s)$, the density in cold, dense gas clouds, is only weakly constrained by direct observation, because the hypothetical clouds constitute a form of *dark* matter. We therefore proceed by adopting a conventional dark matter density distribution for the Galaxy, namely a cored isothermal sphere, as our model cloud density distribution, with a fiducial normalisation which is equivalent to the assumption that all of the dark matter is in the form of dense gas clouds. This corresponds to the model

$$\rho = \frac{\sigma^2}{2\pi G(R^2 + z^2 + r_c^2)}, \qquad (5)$$

in terms of cylindrical coordinates (R, z), with $\sigma = 155$ km s^{-1}. We have adopted a core radius of $r_c = 6.2$ kpc based on the preferred model of Walker (1999). (This choice corresponds to Walker's preferred value of cloud column density $\Sigma = 140\,\mathrm{g\,cm^{-2}}$.) Walker's model exhibits a core radius which is a function of cloud column density, but we have fixed the core radius at 6.2 kpc for all

of our computations. This choice permits more straightforward consideration of the observational constraints because Q is independent of Σ in this case.

It then remains to specify the cosmic-ray energy-density as a function of position in the Galaxy. Webber, Lee and Gupta (1992) (hereafter WLG92) constructed numerical models of cosmic-ray propagation in the Galaxy; they did not give any analytic forms for their model cosmic-ray distributions, but an appropriate analytic approximation can be deduced from the results which they obtained. They found that the cosmic-ray radial distribution reflects, in large part, the radial dependence of cosmic-ray sources, with a modest smoothing effect introduced by diffusion. We have therefore adopted WLG92's preferred model (their model 3) for the radial distribution of sources as our model for the radial distribution of cosmic rays.

The various spectra of cosmic-ray isotope ratios considered by WLG92 favour models in which the diffusion boundaries are in the range $2 - 4$ kpc above and below the plane of the Galaxy. We adopt the midpoint of this range. WLG92 do not give a simple functional form for the vertical variation of cosmic-ray density within this zone, so we have simply assumed an exponential model: $\exp(-|z|/h)$. We know that in WLG92's models the cosmic-ray density is fixed at zero at the diffusion boundaries, and consequently the scale height of the exponential should be approximately half the distance to the diffusion boundary, i.e. $h \simeq 1.5$ kpc.

These considerations lead us to the model cosmic-ray mean intensity distribution $J_{cr}(R, z)$:

$$\frac{J_{cr}(R, z)}{J_{cr}(\odot)} = \left(\frac{R}{R_0}\right)^{0.6} \exp[(R_0 - R)/L - |z|/h],$$
$$(6)$$

in terms of cylindrical coordinates (R, z). Here $R_0 \simeq 8.5$ kpc is the radius of the solar circle, while $L = 7$ kpc, $h = 1.5$ kpc and $J_{cr}(\odot) = J_{cr}(R_0, 0)$. This distribution has the character of a disk with a central hole.

These models for $\rho(s)$ and J_{cr} allow us to compute the quantity Q, as per equation 4, and the resulting variation over the sky is plotted in figure 8. For reference we give the values of $Q(l, b)$ evaluated at the cardinal points, as follows:

$Q(0,0) = 6.47 \times 10^{-2} \mathrm{g\,cm^{-2}}$, $Q(\pm 90°, 0) = 1.54 \times 10^{-2} \mathrm{g\,cm^{-2}}$, $Q(180°, 0) = 7.70 \times 10^{-3} \mathrm{g\,cm^{-2}}$, and $Q(b = \pm 90°) = 2.44 \times 10^{-3} \mathrm{g\,cm^{-2}}$. In order to compare with the EGRET results of Hunter et al. (1997), we have also evaluated the average of Q over the inner Galactic disk: $\langle Q(|l| \leq 60°, |b| \leq 10°)\rangle = 3.28 \times 10^{-2} \mathrm{g\,cm^{-2}}$.

3. Discussion

3.1. Comparison with data

Several physical processes contribute to the observed diffuse gamma-ray intensity. In order of decreasing fractional contribution these are thought to be pion production and bremsstrahlung from cosmic-ray interactions with *diffuse* Galactic gas, inverse Compton emission from cosmic-ray electrons interacting with ambient photons, and an isotropic background, which is presumably extragalactic and due to many faint, discrete sources. The sum of these contributions offers a good model for the diffuse emission which is actually observed in the 100 MeV–1 GeV band (Bloemen 1989; Hunter et al. 1997); however, the $E > 1$ GeV emission is poorly modeled (Hunter et al. 1997) with the prediction (Bertsch et al. 1993) amounting to only $\sim 2/3$ of the observed intensity.

Some authors (Gilmore 1994; Salati et al. 1996) have used the low-energy ($E < 1$ GeV) data to argue that the agreement between model and data allows no room for any significant unmodeled emission and that these data therefore place tight constraints on any baryonic contribution to the dark matter halo of the Galaxy. This line of argument is clearly suspect because of the failure of the same model to account for the high-energy ($E > 1$ GeV) data. However, even if we ignore the high-energy data the calculations presented in §2.3 demonstrate that the gamma-ray constraints on high column density gas clouds in the dark halo are much weaker than those on low column density gas because the emissivity of the latter is much greater; consequently, we revisit the published constraints in the following section (§3.2), returning to the question of the high-energy data in §3.3.

3.2. Published constraints applied to high column-density gas

Gilmore (1994) argued that the known (diffuse)

gas accounts for essentially all of the gamma-ray intensity in the $E > 100$ MeV band observed by the COS B satellite (Bloemen 1989), and he suggested that any contribution from baryonic clouds should amount to no more than $10^{-5} \mathrm{ph\,cm^{-2}s^{-1}sr^{-1}}$ ($E > 100$ MeV) at high Galactic latitudes. Toward the Galactic poles we found (§3) $Q \simeq 2.5 \times 10^{-3} \mathrm{g\,cm^{-2}}$, implying that the average emissivity of the material in the dark halo should be $\mathcal{E} < 5.0 \times 10^{-2} \mathrm{ph\,s^{-1}g^{-1}}$ for $E > 100$ MeV. From Table 1 (or figures 6 and 7) we see that this requirement is not met for the models which are in the thin material limit but that any model with $\Sigma \gtrsim 100 \mathrm{g\,cm^{-2}}$ is acceptable. In other words the constraint imposed by Gilmore (1994) permits the Galaxy's dark halo to be entirely baryonic, provided the individual components have a column-density $\Sigma \gtrsim 100 \mathrm{g\,cm^{-2}}$.

Salati et al. (1996) pointed out that obervations at low Galactic latitudes can provide tighter constraints on any baryonic dark halo, because of the higher intensity expected when looking through the cosmic-ray disk edge-on. This point is manifest in the large values of $Q(b = 0)$, which we computed in §2.3 (see also figure 8). Salati et al. (1996) argued that a suitable constraint on any baryonic component of the dark halo is that it should not contribute more than the uniform background intensity component observed in any given field. The strongest constraint then comes from observations of the Ophiuchus region (Hunter et al. 1994), for which the requirement imposed by Salati et al. (1996) is an intensity contribution from the dark matter halo of $I_D < 2.4 \times 10^{-6} \mathrm{ph\,cm^{-2}s^{-1}sr^{-1}}$ in the band 300 MeV $\leq E \leq 500\$ MeV. For this line of sight our calculation yields $Q(0, b = 15°) = 1.66 \times 10^{-2} \mathrm{g\,cm^{-2}}$, and in the thin material limit, for which we find $\mathcal{E} \simeq 2.4 \times 10^{-2} \mathrm{ph\,s^{-1}g^{-1}}$ (300 MeV $\leq E \leq 500\$ MeV; see Table 1), this corresponds to a predicted intensity of $I_D \simeq 3.2 \times 10^{-5} \mathrm{ph\,cm^{-2}s^{-1}sr^{-1}}$ in the 300–500 MeV band, implying that at most 8% of the dark halo can be resident in low column density clouds.[2] However, our calculations extend to

---

[2]This result is a factor of 2 larger than the corresponding model of Salati et al. (1996) (with $L = 3$ kpc and a spherical halo), a difference which is accounted for by their choice of a smaller core radius for the dark halo. Salati et al. (1996) chose a core radius of 3.5 kpc, which yields $Q(0, b = 15°) = 3.0 \times 10^{-2} \mathrm{g\,cm^{-2}}$, whereas we have em-

clouds of higher column-densities, and we find that for $\Sigma \gtrsim 500\,\mathrm{g\,cm^{-2}}$ the limit relaxes to the point where all of the dark halo is permitted to be in the form of high column density clouds.

3.3. Revision of constraints based on the observed spectrum

3.3.1. *Galactic diffuse gamma-ray model*

The constraints discussed in the previous subsection make reference only to the low-energy ($E < 1$ GeV) gamma-ray data. As noted earlier in this section, the observed intensity of the inner Galactic disk at high photon energies (> 1 GeV) is substantially greater than expected (Hunter et al. 1997; Bertsch et al. 1993). Much effort has been expended on explaining this discrepancy, with most of the attention given to models in which the Galactic cosmic-ray electron and/or proton spectra differ from their locally measured values (Büsching, Pohl & Schlickeiser 2001; Aharonian & Atoyan 2000; Berezhko & Völk 2000; Strong, Moskalenko and Reimer 2000; Mori 1997). However, none of these models offers a satisfactory explanation of the observed mean gamma-ray spectrum of the Galactic disk, and consequently a successful match to the low energy data should not be taken to mean that the emission model is correct. In turn this suggests that the constraints formulated by Gilmore (1994) and Salati et al. (1996), on the basis of the low-energy data, may be too restrictive.

The question then arises as to what constraints the gamma-ray data do in fact place on unmodeled emission, given the current state of understanding of the observed emission.

The Galactic diffuse emission model used in Hunter et al. (1997) is based on Bertsch et al. (1993), and contains the following contributions:

$$I = I_{\mathrm{HI}} + I_{\mathrm{HII}} + I_{\mathrm{H_2}} + I_{\mathrm{IC}} + I_{\mathrm{EG}}, \qquad (7)$$

where I_{HI} is the gamma-ray intensity contributed by cosmic-ray interactions with diffuse atomic hydrogen, and similarly for the ionised and molecular components of the interstellar medium (HII and $\mathrm{H_2}$, respectively). The emissivity for these components (Bertsch et al. 1993) is, of course, computed in the thin material limit, and each compo-

 nent therefore has the same spectral shape, differing only in normalisation. Here I_{IC} is the gamma-ray flux by inverse Compton emission (cosmic-ray electrons up scattering low-energy photons), and I_{EG} is the isotropic extragalactic background flux.

Although the atomic and ionised hydrogen components can be observed directly via their line emission, and are thus well constrained, this is not true for the molecular component. The molecular hydrogen column is assumed to be proportional to the CO emission line strength, as measured by the Columbia CO survey (Dame et al 1987), for example, but the constant of proportionality (usually denoted by X) is unknown and one is forced to determine its value by fitting to the gamma-ray data. Although the uncertainty in the best-fit determination of $\langle X \rangle$ (averaged over the whole sky) is small, the systematic uncertainties are acknowledged to be much larger, "at least 10%–15%" (Hunter et al. 1997). In turn, this estimate of the uncertainty is small in comparison with the differences among the various values of X which have been reported in the literature (see the review by Bloemen (1989)) and the likely range of variation in X within the Galaxy (Hunter et al. 1997). Although these are substantial uncertainties, molecular hydrogen contributes only a fraction of the total observed gamma-ray intensity roughly 20% of the local surface density of gas in the Galactic disk is thought to be in molecular form (Wouterloot et al 1990) so the implied fractional uncertainty in the total Galactic emission is perhaps as small as 3%. Moreover, uncertainty in X affects only the normalisation and not the spectral shape of the predicted emission from diffuse molecular hydrogen, so the observed high-energy excess cannot be explained in this way even if X could assume an arbitrarily large value.

The other main contributions to uncertainty in the diffuse model are associated with (1) unmodeled spatial variations in the cosmic-ray spectral energy density and (2) unmodeled spatial variations in the low-energy photon spectral energy density; the former affects all of the Galactic contributions to I, whereas the latter affects only the inverse Compton component. These uncertainties affect both the normalisation and the spectral shape of the predicted gamma-ray emission; however, the uncertainties are difficult to quantify.

---

ployed a core radius of 6.2 kpc (see §2.3).

3.3.2. Constraints based on the gamma-ray data

For our purposes it is not actually necessary to quantify the uncertainties on the model input parameters; it suffices to use the discrepancy between model and data as a measure of the uncertainty in our understanding of the observed emission. In turn this measure determines the constraints which we can apply to any putative unmodeled emission, such as the contribution from dense gas which we are concerned with here. At photon energies $E > 1$ GeV the fractional discrepancy is roughly 60% (Hunter et al. 1997), in the sense that the observed emission is 1.6 times larger than the model, and we henceforth adopt $0.6/1.6 \simeq 40\%$ of the total observed intensity as our estimate of the unmodeled emission. Although this estimate is derived from data at high energies, the effects of the various contributing processes are all very widely spread, and *the estimate therefore applies independent of photon energy.* The constraints appropriate to high/low Galactic latitudes can now be re-evaluated.

At high Galactic latitudes the observed intensity is $I \simeq 1.5 \times 10^{-5} \, \mathrm{ph \, cm^{-2} s^{-1} sr^{-1}}$ for $E \geq 100$ MeV (Kniffen et al. 1996), implying that any unmodeled emission should be $\lesssim 6 \times 10^{-6} \, \mathrm{ph \, cm^{-2} s^{-1} sr^{-1}}$ in this band. This result is actually slightly stricter than the criterion used by Gilmore (1994) and thus leads us to tighten our high-latitude constraints, relative to those quoted in §3.2: the observed high-latitude gamma-ray intensity constrains the amount of low column-density gas to $\lesssim 20\%$ of the total density of the Galactic dark halo, with this fraction rising to 100% for gas clouds of column density $\Sigma \gtrsim 200 \, \mathrm{g \, cm^{-2}}$.

At low Galactic latitudes we can make use of the mean intensity of the inner Galactic disk, which has been accurately determined by Hunter et al. (1997). For example at 1 GeV the mean intensity ($|l| \leq 60°$, $|b| \leq 10°$) is $\langle I \rangle \simeq 3 \times 10^{-8} \, \mathrm{ph \, cm^{-2} s^{-1} sr^{-1} MeV^{-1}}$, and our calculation of $\langle Q \rangle$ for this region yields (§2.3) $3.28 \times 10^{-2} \, \mathrm{g \, cm^{-2}}$, implying that the emissivity of the Galactic dark halo material must be, on average, $\mathcal{E} \leq 4.6 \times 10^{-6} \, \mathrm{ph \, s^{-1} g^{-1} MeV^{-1}}$. By comparison, the actual emissivity of low column-density gas is computed to be (§2.3, table 2) $\mathcal{E}(1 \, \mathrm{GeV}) \simeq 1.4 \times 10^{-5} \, \mathrm{ph \, s^{-1} g^{-1} MeV^{-1}}$, imply-

ing that $\lesssim 30\%$ of the Galaxy's dark halo may be comprised of low column density gas. For higher column densities the emissivity falls, and table 2 shows that for $\Sigma = 100 \, \mathrm{g \, cm^{-2}}$ the emissivity is only $5.5 \times 10^{-6} \, \mathrm{ph \, s^{-1} g^{-1} MeV^{-1}}$. The gamma-ray data on the inner Galactic disk thus indicate all of the Galaxy's dark halo to be made of dense clouds of column-density $\Sigma \gtrsim 100 \, \mathrm{g \, cm^{-2}}$.

3.4. Comment on the gas content of the galactic disk

The constraint we have just given is based on the mean spectrum of the inner Galactic disk, in contrast to those given by Salati et al. (1996) who employed limits based on the angular structure of the observed gamma-ray intensity. Specifically, Salati et al. (1996) required that the putative contribution of emission from a baryonic component of the Galaxy's dark halo be less than that of the isotropic component of the observed intensity; this procedure seems to us to be less reliable than the procedure we have employed, for two reasons. First, even if the dark halo were spherically symmetric the emission from any baryonic component would not be, both because our point of observation is quite distant from the centre of the Galaxy and because the resulting gamma-ray emission is strongly dependent on the Galactic cosmic-ray distribution, which in turn is strongly concentrated in the disk of the Galaxy. Indeed the cosmic-ray distribution appears to correlate with the distribution of interstellar matter (Hunter et al. 1997), thus complicating the interpretation of the observed gamma-ray intensity distribution. In particular this coupling leads to gamma-ray emission from a baryonic dark halo being correlated with the diffuse gas column density, even if the dense gas is uncorrelated with the diffuse gas. Second, on any given line of sight, such as the Ophiuchus field considered by Salati et al. (1996), a highly structured dark matter halo might exhibit, by chance, a low dark matter column density. The chances of this are good if, as in the case of Salati et al. (1996), the field is specifically chosen to have a low "background" intensity.

4. Summary

The gamma-ray spectra arising from cosmic-ray interactions with gas clouds of various column-

densities have been calculated using a Monte Carlo event simulator, GEANT4. Our calculations reproduce the analytic result in the low column-density limit, where only single particle interactions need to be considered, but exhibit significant differences for clouds of column-density $\Sigma \gtrsim 10^2 \, \mathrm{g \, cm^{-2}}$ where the emissivity declines substantially for photon energies $E \gtrsim 100$ MeV. The low emissivity of dense gas means that the baryonic content of the Galaxy's dark halo is not so tightly constrained by the gamma-ray data as had previously been thought. For $\Sigma \gtrsim 200 \, \mathrm{g \, cm^{-2}}$ we find that the existing gamma-ray data, taken in isolation, do not exclude purely baryonic models for the Galactic dark halo.

We are grateful to the referee for constructive comments that have improved this paper.

REFERENCES

Aharonian, F. A., & Atoyan, A.M. 2000 A&A, 362, 937

Asakimori, K. et al. 1998, ApJ, 502, 278

Barwick, S. W. et al. 1998, ApJ, 498, 779

Berezhko, E.G., & Völk, H.J. 2000, ApJ, 540, 923

Bertsch, D.L. et al. 1993, ApJ, 416, 587

Bloemen H. 1989, ARA&A, 27, 469

Boezio, M. et al. 1999, ApJ, 518, 457

Boezio, M. et al. 2000, ApJ, 532, 653

Büsching, I., Pohl, M., & Schlickeiser, R. 2001 A&A, 377, 1056

Casadei, D., & Bindi, V. astro-ph/0302307

Cavallo, G., & Gould, R. J. 1971, Nuovo Cimento, 2B, 77

Combes, F. & Pfenniger, D. 1997, A&A, 327, 453

Dame, T. M. et al. 1987, ApJ, 322, 706

Dannheim, D. "Test of π^0-production in Geant4", CERN Summer Student Report, 15 September 1999 (unpublished: available at CERN website)

De Paolis, F. et al. 1995, Phys. Rev. Lett., 74, 14

Dermer, C.D. 1986, A&A, 157, 223

Fiedler, R. et al. 1994, ApJ, 430, 581

Fukugita M. 2004, in IAU Symp. 220, in press (astro-ph/0312517)

Gaisser, T. K. & Shaefer, R. K. 1992, ApJ, 394, 174

Gerhard, O. & Silk, J. 1996, ApJ, 472, 34

Gilmore, G. 1994, ApJS, 92, 539

Golden, R. L. et al. 1984, ApJ, 287, 622

Golden, R. L. et al. 1994, ApJ, 436, 769

Hartman et al. 1999, ApJS, 123, 79

Henriksen R. N., & Widrow L. M. 1995, ApJ, 441, 70

Hunter, S.D., Digel, S.W., de Geus, E.J., & Kanbach G. 1994 ApJ 436, 216

Hunter, S.D. et al. 1997, ApJ, 481, 205

Ivanenko, I. P. et al. 1993, in Proc. of the 23rd International Cosmic Ray Conference, Calgary, 2, 17

Kalberla, P.M.W., Shchekinov, Yu.A. & Dettmar, R.-J. 1999 A&A, 350, L9

Kawamura, Y. et al. 1989, Phys. Rev. D, 40, 729

Kniffen D.A. et al. 1996 A&A, Suppl. 120, 615

Kobayashi, T. et al. 1999, Proc. 26th Int. Cosmic-Ray Conf. (Salt Lake City), 3, 61

McKee, C.F. 2001 ASP Conf Ser 243, 155

Mori, Masaki 1997, ApJ, 478, 225

Moskalenko, I.V. & Strong, A.W. 1998 ApJ, 493, 694

Pfenniger, D., Combes, F., & Martinet, L. 1994, A&A, 285, 79

Ryan, M. J. et al. 1972, Phys. Rev. Lett., 28, 985

Salati, P., Chardonnet, P., Luo, X., Silk, J., & Taillet, R. 1996 A&A, 313, 1

Sanuki, T. et al., 2000, ApJ, 545, 1135

Sciama, D.W. 2000a, MNRAS, 312, 33

Sciama, D.W. 2000b, MNRAS, 319, 1001

Seo, E. S. et al. 1991, ApJ, 378, 763

Shikaze, Y. 2001, Ph.D. thesis, University of Tokyo

Skibo, J.G. and Ramaty, R. 1993, A&A Suppl., 97, 145

Smith, L. H. et al. 1973, ApJ, 180, 987

Stephens, S.A. & Badhwar, G.D. 1981, Ap&SS, 76, 213

Strong, A.W., Moskalenko, I.V. & Reimer, O. 2000, ApJ, 537, 763

Tang, K.-K., ApJ, 1984, 278, 881

Torii, S. et al., ApJ, 2001, 559, 973

Umebayashi, T. & Nakano, T., PASJ, 1981, 33, 617

Walker, M. & Wardle, M., 1998, ApJ, 498, L125

Walker, M. 1999, MNRAS, 308, 551

Walker, M., Mori, M. & Ohishi, M. 2003, ApJ, 589, 810

Wardle, M. & Walker, M. 1999, ApJ, 527, L109

Webber, W. R. et al. 1987, in Proc. of the 20th International Cosmic Ray Conference, Moscow, 1, 325

Webber, W.R., Lee, M. & Gupta, M. 1992 ApJ390, 96 (WLG92)

Wouterloot, J.G.A., Brand, J., Burton, W.B., & Kwee, K.K. 1990 A&A230, 21

Fig. 1.— Adopted cosmic-ray proton spectrum in the Galaxy. The model curves are taken from Mori (1997) and Shikaze (2001). Also plotted are direct observations of the local spectrum (Ryan et al. 1972; Smith et al. 1973; Webber et al. 1987; Kawamura et al. 1989; Seo et al. 1991; Ivanenko et al. 1993; Asakimori et al. 1998; Boezio et al. 1999; Sanuki et al. 2000), but note that these are strongly affected by solar modulation.
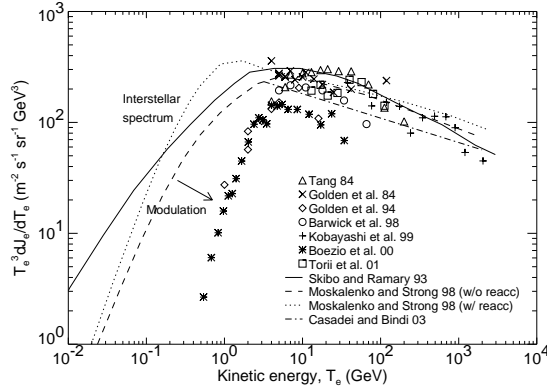

Fig. 2.— Adopted cosmic-ray electron spectrum in the Galaxy. The model curves are taken from Skibo and Ramaty (1993), Moskalenko and Strong (1998) and Casadei and Bindi (2003). (The two lines for Moskalenko and Strong (1998) show models with and without reacceleration of the cosmic rays.) Also plotted are direct observations of the local electron spectrum (Tang 1984; Golden et al. 1984, 1994; Barwick et al. 1998; Kobayashi et al. 1999; Boezio et al. 2000; Torii et al. 2001), but note that these are affected by solar modulation.
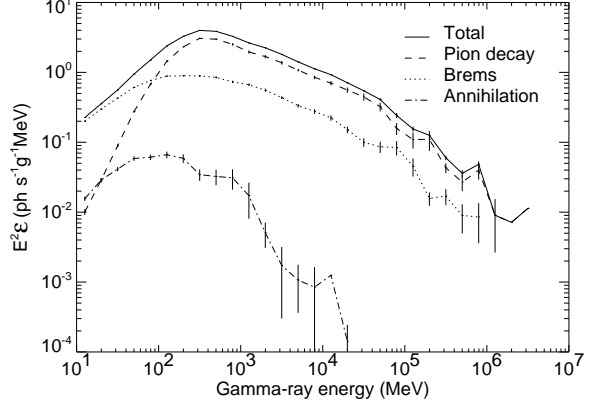

Fig. 3.— Gamma-ray emissivity, $E^2\mathcal{E}$, for a molecular hydrogen cloud, of radius 1 AU and column density $100\,\mathrm{g\,cm^{-2}}$, irradiated by cosmic-ray protons; vertical bars represent Monte Carlo statistical errors. The various contributing emission processes are also shown separately.
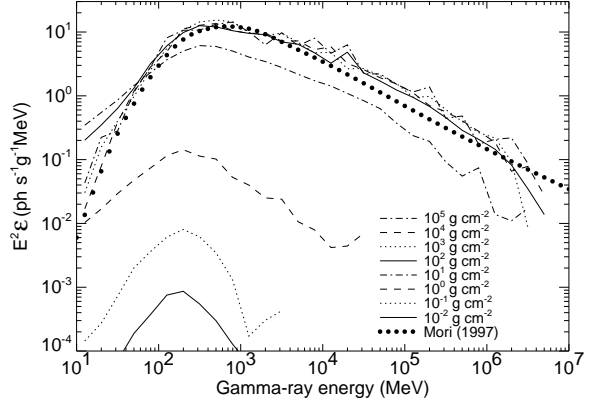

Fig. 4.— Gamma-ray emissivities for dense clouds irradiated by cosmic-ray protons, with a spectrum appropriate to the solar neighbourhood. The results have been multiplied by a nuclear enhancement factor of 1.52 (Mori 1997) to account for the presence of heavier nuclei in the cosmic-rays. The different curves are for various different column-densities: $10^{-2}\,\mathrm{g\,cm^{-2}}$, thick dot-dashed curve; $10^{-1}\,\mathrm{g\,cm^{-2}}$, thick dashed curve; $1\,\mathrm{g\,cm^{-2}}$, thick dotted curve; $10\,\mathrm{g\,cm^{-2}}$, thick solid curve; $10^2\,\mathrm{g\,cm^{-2}}$, thin dot-dashed curve; $10^3\,\mathrm{g\,cm^{-2}}$, thin dashed curve; $10^4\,\mathrm{g\,cm^{-2}}$, thin dotted curve; $10^5\,\mathrm{g\,cm^{-2}}$, thin solid curve. Also plotted is the emissivity from Mori (1997), which corresponds to the "thin material" limit (filled circles); this limit offers a good approximation for $\Sigma \lesssim 10\,\mathrm{g\,cm^{-2}}$.
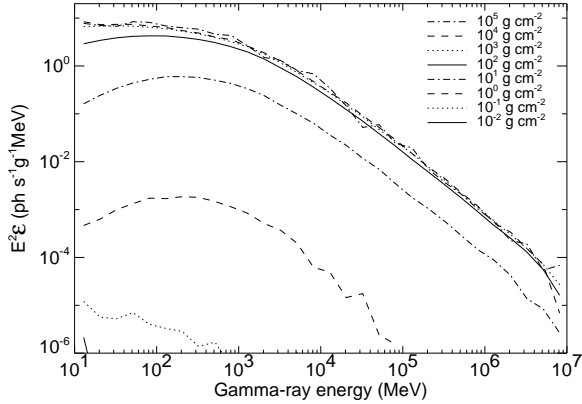
Fig. 5.— Gamma-ray emissivities for dense clouds irradiated by cosmic-ray electrons. The different curves are for different column-densities, as per figure 4.
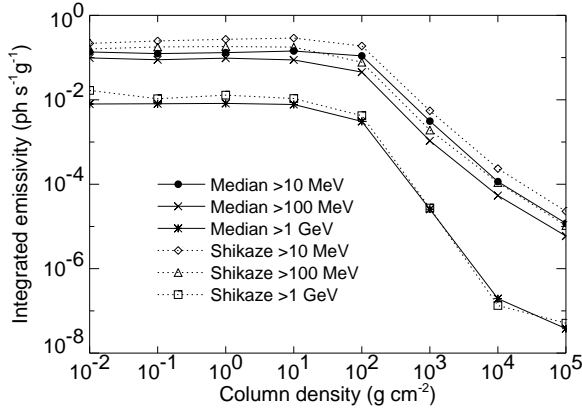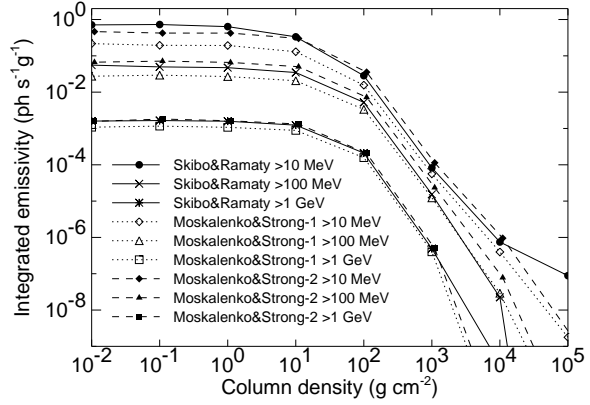

Fig. 7.— Integrated gamma-ray emissivities for dense clouds irradiated by cosmic-ray electrons. Solid curves are those assuming a cosmic ray electron flux in Skibo and Ramaty (1993), and dashed (dotted) ones assuming that in Moskalenko and Strong (1998) with (without) re-acceleration.

Fig. 6.— Integrated gamma-ray emissivities for dense clouds irradiated by cosmic-ray hadrons. Solid curves are those assuming a cosmic ray proton flux in Mori (1997) and dotted ones assuming that in Shikaze (2001). Here we multiplied by a nuclear enhancement factor of 1.52 (Mori 1997) to take account of heavy nuclei in the cosmic rays.
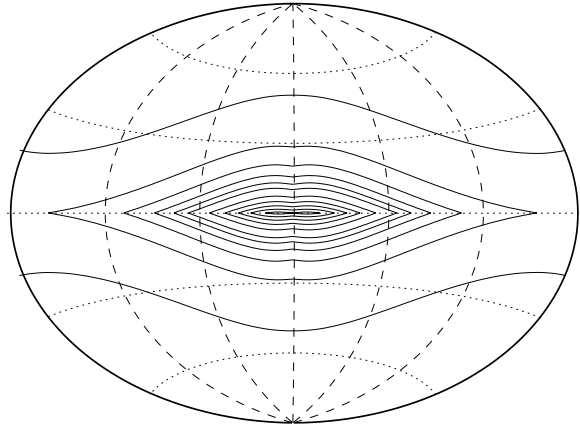

Fig. 8.— Adopted model dark matter column-density distribution over the sky, $Q(l, b)$, weighted by cosmic-ray energy density and displayed in Galactic coordinates. The quantity Q is defined in equation 4 and is computed using the dark matter density model given in equation 5 together with the cosmic-ray distribution model given in equation 6. Contour levels are $(4, 8, 12, 16, 20, 24, 32, 40, 48, 56, 64) \times 10^{-3}\,\mathrm{g\,cm^{-2}}$; dashed lines are constant longitude, spaced at $60°$ intervals; dotted lines are constant latitude, spaced at $30°$ intervals .